JOURNAL OF GEOPHYSICAL RESEARCH, VOL. 113, D00C13, doi:10.1029/2008JD009903, 2008

Regional variability of the composition of mineral dust from western Africa: Results from the AMMA SOP0/DABEX and DODO field campaigns

P. Formenti,[1] J. L. Rajot,[2] K. Desboeufs,[1] S. Caquineau,[3] S. Chevaillier,[1] S. Nava,[4] A. Gaudichet,[1] E. Journet,[1] S. Triquet,[1] S. Alfaro,[1] M. Chiari,[4] J. Haywood,[5] H. Coe,[6] and E. Highwood[7]

Received 1 February 2008; revised 9 June 2008; accepted 22 July 2008; published 24 October 2008.

[1] This paper presents data on elemental and mineralogical composition of mineral dust from various source regions of Africa collected during the African Monsoon Multidisciplinary Analyses (AMMA) SOP0/DABEX and Dust Ouflow and Deposition to the Ocean (DODO) DODO1 experiments (January–February 2006), and the DODO2 campaign (August 2006). Bulk filter samples were collected at the AMMA supersite of Banizoumbou, Niger, as well as on board the Facility for Airborne Atmospheric Measurements (FAAM) BAe-146 aircraft. Both mineral dust and biomass burning in external mixing occurred in surface and elevated layers during the winter field phase of the campaign. However, mineral dust was overwhelming, accounting for 72% of the estimated aerosol mass in aged elevated biomass burning layers and up to 93% in plumes of mineral dust, which generally occurred in the boundary layer. A number of well-defined episodes of advection of mineral dust could be identified both at the ground and on the aircraft. The elemental and mineralogical composition varied depending on source region. This variability could be well traced by the calcium content, which is enhanced in dust from North Africa but depleted in dust from the Sahel. Iron oxides in the form of hematite and goethite are enriched in dust emitted within Sahel and in Mauritania, whereas dust from the Bodélé depression is iron-oxide depleted. Iron oxides represented between 2.4% and 4.5% of the total estimated dust oxide mass. This regional variability will have to be taken into account in estimating the optical properties of absorption of mineral dust from western Africa.

Citation: Formenti, P., et al. (2008), Regional variability of the composition of mineral dust from western Africa: Results from the AMMA SOP0/DABEX and DODO field campaigns, *J. Geophys. Res.*, *113*, D00C13, doi:10.1029/2008JD009903.

1. Introduction

[2] Mineral dust is an important aerosol species both in terms of emissions and climatic impact [*Forster et al.*, 2007]. Dust particles have diameters up to several microns and a nonzero imaginary part of the refractive index, thus they are able to scatter and absorb both the solar and terrestrial radiation, and modify the solar and the infrared radiative budget at the surface and top of the atmosphere [*Sokolik et al.*, 2001]. Additional effects of mineral dust on climate concern the cloud radiative and physical properties, and the hydrological cycle [*Ramanathan et al.*, 2001], the modification of the atmospheric gaseous composition through heterogeneous reactions [*Dentener et al.*, 1996; *de Reus et al.*, 2000; *Salisbury et al.*, 2006], and the transport of nutrients to the sea surface water and the Amazon forest [*Swap et al.*, 1992; *Jickells et al.*, 2005]. All these climatic effects depend on the mineralogical composition of mineral dust, in particular on the content and mineralogy of clays and iron oxides [*Sokolik and Toon*, 1999; *Lafon et al.*, 2006; *Jickells et al.*, 2005; *Hudson et al.*, 2008].

[3] This paper presents data on the elemental and mineralogical composition of African mineral dust aerosols collected in the framework of three of the field campaigns of the African Monsoon Multidisciplinary Analyses (AMMA) project [*Redelsperger et al.*, 2006] and the Dust Ouflow and Deposition to the Ocean (DODO) experiment [*McConnell et al.*, 2008]. Numerous previous studies have shown that the mineralogical composition of African mineral dust varies depending on the source region of emission [*Caquineau et al.*, 1997, 2002; *Moreno et al.*, 2006].

[1] LISA, Universités Paris 12 et Paris 7, CNRS, Créteil, France.
[2] UR 176 Solutions, Institut de Recherche pour le Développement, Niamey, Niger.
[3] UR 055 Paleotropique, Institut de Recherche pour le Développement, Bondy, France.
[4] National Institute of Nuclear Physics, Florence, Italy.
[5] Met Office, Exeter, UK.
[6] School of Earth, Atmosphere and Environmental Science, University of Manchester, Manchester, UK.
[7] Department of Meteorology, Reading University, Reading, UK.

0148-0227/08/2008JD009903$09.00

[4] These studies looked mainly at the clay content and mineralogy. However, to date no field data exist on the regional variability of the iron oxide content, and mineralogy, despite of their potential effect on the optical properties of mineral dust [*Claquin et al.*, 1999; *Sokolik and Toon*, 1999]. Iron oxides and hydroxides such as hematite (Fe_2O_3) and goethite (FeO-OH) are known to absorb radiation in the visible spectrum, but with different intensity and at different wavelengths [*Sokolik and Toon*, 1999; *Lafon et al.*, 2006]. In order to estimate correctly the complex part of the dust refractive index, thus their absorption properties, both the content and the mineralogy of the iron oxides have to be determined.

[5] This paper aims to fill this gap. We present here elemental and mineralogical analysis of samples collected over Niger in wintertime (January–February 2006), when biomass burning emissions around the gulf of Guinea are also intense, and mixing between mineral dust and biomass burning particles can occur, as well as over Senegal in summertime (August 2006). At this time of the year the biomass burning source is not active in the northern hemisphere [see *Haywood et al.*, 2008, Figure 1]. Mixing with concurrent aerosol species during transport might alter the physico-chemical and optical properties of mineral dust, and therefore must be taken into account when assessing its direct radiative impact at the regional scale.

[6] In this paper we will address the following questions:

[7] 1. What is the respective contribution of mineral dust and biomass burning to the atmospheric aerosol load in western Africa?

[8] 2. Which is the elemental and mineralogical composition of mineral dust? In particular, what is the iron oxide content and mineralogy?

[9] 3. Are there any indications that the elemental and mineralogical composition vary at the regional scale?

[10] This paper completes the body of observations of mineral dust presented by *Rajot et al.* [2008], *Osborne et al.* [2008], *Chou et al.* [2008] and *McConnell et al.* [2008].

2. Method

[11] Wintertime measurements have been performed at the ground-based AMMA supersite of Banizoumbou in Niger (13.5°N 2.6°E, 250 m above sea level) as well as on board the Facility for Airborne Atmospheric Measurement (FAAM) BAe-146 research aircraft. The aircraft was based in Niamey (Niger) in January (this phase of the airborne campaign is known as Dust and Biomass Experiment (DABEX)) and Dakar (Senegal) in February for DODO1. Additional aircraft data were collected in summertime (21–29 August 2006) during the second phase of the DODO experiment (DODO2), when the aircraft was again based in Dakar (Senegal).

2.1. Aerosol Filter Sampling

2.1.1. Airborne Sampling

[12] Instruments and samplers were operated on board the Facility for Airborne Atmospheric Research (FAAM) BAe-146 research aircraft. The regions of operation of the aircraft during the AMMA SOP0/DABEX and DODO experiments are presented by *Haywood et al.* [2008] and *McConnell et al.* [2008].

[13] The full description of the aircraft and onboard instrumentation is also provided in *Haywood et al.* [2008]. Here, we limit our discussion to the aerosol sampling system for filter collection. The filter lines on board the BAe-146 are the same that previously used on board the UK MetOffice C-130 on various field campaigns (e.g., the Saharan Dust Experiment (SHADE) [*Tanré et al.*, 2003]) and are described in detail by *Andreae et al.* [2000]. The aerosol inlet consists of a thin-walled inlet nozzle with a curved leading edge; the design was based on criteria for aircraft engine intakes at low Mach numbers [*Andreae et al.*, 1988]. This design reduces distortion of the pressure field at the nozzle tip and the resulting problems associated with flow separation and turbulence. The sampling system operated at flow rates that averaged 120 L min^{-1} (at ambient pressure and temperature); the flow was adjusted to maintain slightly subisokinetic sampling conditions. The aerosol intake system was designed so that rain and large cloud water droplets would be removed from the sampled air stream by inertial separation. The passing efficiency of the inlets has not been quantified. However, *Chou et al.* [2008] has shown that the number size distributions of the aerosols collected on the filters (counted by electron microscopy) extended up to 10 μm diameters and were comparable to those measured by wing-mounted optical counters.

[14] Aerosol particles were sampled by filtration onto two stacked-filter units (SFUs) mounted in parallel. Each SFU can hold a maximum of three filters on sequential 47-mm diameter polyethylene supports, but only one stage was used during AMMA SOP0/DABEX. Samples were collected only during horizontal flight legs lasting not less than 20–30 min in order to guarantee sufficient loading of the filter samples. Each SFU consisted of a Nuclepore filter of nominal pore size 0.4 μm. One SFU was used for measuring water-soluble ions and major, minor, and trace elements. The second SFU was used for measuring carbonaceous aerosols. In this case the sampling medium consisted of one Whatman QMA quartz filter. Quartz filters were pre-baked at 600°C for approximately 12 h to eliminate organic impurities.

[15] Blank samples were collected on every flight by placing filters in the sampling line as if they were actual samples, and exposing them to the air stream for a few seconds. Immediately after each flight, loaded and blank filters were stored in Petri dishes. Back in the laboratory, the 90-mm Nuclepore filter samples were cut in sub-portions of various surface areas (from one eighth up to one half of the filter) to be submitted to different types of analysis. Details are provided in section 2.2. After decarbonatation by HCl fumes, the quartz filters was analyzed to yield the non-dust carbon (TC) content of the aerosols.

[16] In total, 99 Nuclepore filter samples have been collected during the 24 research flights of the BAe-146; 13 research flights were performed from Niamey, Niger during DABEX/AMMA SOP-0, two scientific transit flights were performed from Niamey to Dakar and 12 flights from Dakar, Senegal during the wintertime DODO1 and summertime DODO2 campaigns.

2.1.2. Ground-Based Sampling

[17] Ground-based measurements have been performed at the AMMA super site of Banizoumbou (13.5°N 2.6°E, 250 m above sea level), Niger. This station is located at a remote location at about 60 km east of Niamey. A full

description of the sampling site and instrumental set up is provided by *Rajot et al.* [2008].

[18] Aerosol sampling was performed using two identical purpose-built wind-oriented inlets designed for the AMMA field campaigns [*Rajot et al.*, 2008]. The cut-off diameter 50% efficiency of these inlets has been calculated to be approximately 40 μm by using the standard formulae of particle losses in inlet and tubing reported by *Willeke and Baron* [1993] and *Hinds* [1982]. Each inlet leads to a sampling chamber containing seven different sampling lines, each of them dedicated to a different instrument. Multiple sampling is very convenient as it allows collecting various filter samples in parallel, differentiated and optimized in terms of sampling medium, exposure interval and flow rate as a function of the analytical technique to be applied. This also results in minimal manipulation of the filters after sampling. Samples were collected on acid washed 37 mm polycarbonate Nuclepore filters (0.4 μm pore size) mounted on plastic rings. Samples were stored in Petri dishes after sampling.

[19] In total, 76 samples have been collected during the whole sampling period (13 January–13 February 2006). Sampling time was of the order of hours, and was varied depending on the aerosol mass concentration measured online by a Tapered Element Oscillating Microbalance (TEOM, Rupprecht and Patashnick, Albany, USA) [*Rajot et al.*, 2008].

2.2. Aerosol Filter Analysis

2.2.1. Total Elemental Concentration

[20] Total elemental concentrations for all the collected samples (ground-based and aircraft) were obtained by two techniques: Wavelength dispersive X-ray fluorescence (WD-XRF) for the ground-based samples; and Particle-Induced X-ray Emission (PIXE) for the aircraft samples. The reason for using different techniques for ground-based and aircraft samples lays on the fact that the WD-XRF sample holder set up could not host the 90-mm aircraft filters, or portions of them. However, WD-XRF was chosen to analyze the ground-based samples for consistency with previous work [*Alfaro et al.*, 2004; *Lafon et al.*, 2006].

[21] WD-XRF analyses have been performed using a PW-2404 spectrometer by Panalytical. Excitation X-rays are produced by a Coolidge tube (I_{max} = 125 mA, V_{max} = 60 kV) with a Rh anode; primary X-ray spectrum can be controlled by inserting filters (Al, at different thickness) between the anode and the sample. Each element was analyzed three times, with specific conditions (voltage, tube filter, collimator, analyzing crystal and detector), lasting 8 to 10 s. Data were collected for 9 elements (Na, Mg, Al, Si, P, K, Ca, Ti, Fe) using SuperQ software. The elemental mass thickness (μg cm^{-2}), that is, the analyzed elemental mass per unit surface, was obtained by comparing the filter yields with a sensitivity curve measured in the same geometry on a set of dust certified geo-standards (ANRT GS-N). These geo-standards were crunched in order to reduce and homogenize the grain size. Then they were deposited at different concentrations (<150 μg cm^{-2}) on Nuclepore filters. The visual inspection of the deposit by electron microscopy suggested that grains are generally smaller than 5 μm diameter. The atmospheric elemental concentrations were finally calculated by multiplying the analyzed elemental mass thickness by the ratio between the analyzed and the collection surfaces of each sample (16 and 28 mm, respectively). This was possible as the aerosol deposit on the filters was rather uniform. Finally, for the AMMA samples, the limit of quantification of the technique ranged between 3 10^{-3} and 13 10^{-3} μg cm^{-2} depending on element.

[22] Because of limitation in the sample-holder geometry of the WD-XRF, all the BAe146 aircraft samples were analyzed by PIXE. PIXE was performed by a proton beam at the 3 MV Tandetron accelerator of the LABEC laboratory of INFN (Florence), with the external beam set-up [*Calzolai et al.*, 2006].

[23] Each sample was irradiated for about 1000 s with a beam intensity ranging from 5 nA to 30 nA, depending on sample load, over a spot of $\sim$2 mm^2. During irradiation, the filter was moved in front of the beam so that most of the area of deposit was analyzed. PIXE spectra were fitted using the GUPIX code [*Maxwell et al.*, 1995] and elemental concentrations were obtained via a calibration curve from a set of thin standards of known areal density within 5% (Micromatter Inc., Arlington, WA).

2.2.2. Aerosol Mineralogy

[24] The identification of major minerals composing mineral dust (quartz, feldspars, clays, and calcite) was performed by X-ray diffraction (XRD) analysis at the Institute de la Recherche pour le Développement (IRD) in Bondy, France. The analytical procedure and semiquantitative treatment are fully described by *Caquineau et al.* [1997], who adapted the sample preparation to low-mass mineral aerosol (load deposited on filter >1500 μg). Particles are first extracted from the filter with deionized water (pH $\sim$ 7.1), then concentrated by centrifugation (25,000 rpm for 1 h) and finally deposited on a pure silicon slide, such a sample-holder exhibiting a very low and smooth XRD background [*Queralt et al.*, 2001].

[25] Analysis was performed using a Siemens D500 diffractometer with Ni-filtered Cu K_α radiation at 40 kV and 30 mA. Samples were scanned from 2° to 70° (2θ) with counting for 10 s every 0.02°θ.

2.2.3. Iron Oxide Content and Mineralogy

[26] The iron oxide content was determined with the adapted CBD-method developed by *Lafon et al.* [2004]. This method is an adaptation for aerosol filters (with typical material mass less than 500 μg) of the classical method of *Mehra and Jackson* [1960] for soil analysis. The method uses the CBD reagent to dissolve iron oxides selectively via reduction. The remaining iron, called structural iron, occurs in the crystal lattice of silicates and is supposed not contribute to the absorption of visible light [*Faye*, 1968; *Karickhoff and Bailey*, 1973].

[27] The speciation of the mineralogy (identification of hematite and goethite) was performed by diffuse reflectance spectrometry (DRS). Dust aerosol samples were transferred from the polycarbonate filters to a white Teflon plate. Measurements were carried out at room temperature with a Cary 5G UV-VIS-NIR spectrophotometer at the Institute of Institut de Minéralogie et de Physique des Milieux Condensés (IMPMC), Paris, France. The spectrophotometer is equipped with a 110-mm diameter integrating sphere coated with Halon (Labsphere, Inc.). Analyses were performed for spectra in the range from 350 to 1200 nm with a

Table 1. Mean Elemental Concentrations and Mean Elemental Ratios to Al[a]

	Concentrations (μg m^{-3})			
	Ground-Based[b]	Airborne[c]		
	Banizoumbou (Jan–Feb 2006)	AMMA SOP0/DABEX (Jan–Feb 2006)	DODO1 (Feb 2006)	DODO2 (Aug 2006)
Na	1 (1.0)	2 (1)	4 (4)	8 (14)
Mg	3 (1.5)	3 (2)	4 (5)	12 (25)
Al	18 (9)	17 (19)	9 (10)	66 (162)
Si	48 (25)	48 (48)	24 (29)	172 (415)
P	0.2 (0.1)	—	—	—
S	—	2 (1)	4 (5)	3 (6)
K	3 (2)	5 (4)	3 (4)	19 (46)
Ca	6 (4)	9 (9)	9 (19)	36 (82)
Ti	1.4 (0.6)	2 (2)	1 (1)	6 (15)
Fe	10 (5)	10 (11)	6 (8)	45 (109)
	Ratios to Al			
	Ground-Based[b]	Airborne[c]		
	Banizoumbou (Jan–Feb 2006)	AMMA SOP0/DABEX (Jan–Feb 2006)	DODO1[c] (Feb 2006)	DODO2 (Aug 2006)
Na	0.05 (0.04)	0.06 (0.03)	0.5 (0.7)	0.3 (0.6)
Mg	0.14 (0.03)	0.2 (0.1)	0.3 (0.1)	0.2 (0.1)
Al	—	—	—	—
Si	2.7 (0.3)	3.0 (0.6)	2.7 (0.2)	2.7 (0.4)
P	0.012 (0.002)	—	—	—
S	—	0.2 (0.3)	0.1 (0.1)	0.1 (0.3)
K	0.20 (0.05)	0.3 (0.2)	0.2 (0.1)	0.24 (0.06)
Ca	0.4 (0.1)	0.5 (0.3)	0.6 (0.6)	0.6 (0.2)
Ti	0.08 (0.01)	0.10 (0.04)	0.1 (0.1)	0.08 (0.01)
Fe	0.59 (0.06)	0.7 (0.3)	0.70 (0.08)	0.68 (0.04)

[a]Mean elemental concentrations (in μg m^{-3}) obtained from filter sampling at the ground-based site of Banizoumbou and on board the BAe-146 during the AMMA SOP0/DABEX, DODO1, and DODO2 field phases. Mean elemental ratios to Al are also reported. The standard deviation of the each mean value is shown in parentheses.
[b]Seventy-six samples.
[c]Ninety-nine samples.

step of 0.5 nm. The identification of hematite and goethite was done thanks to their absorption bands at around 565 nm and 435 nm, respectively. Following *Scheinost et al.* [1998], by taking the amplitude of the second derivative of the diffuse reflectance signal, we could determine a relative mass fraction of hematite and goethite.

3. Results

3.1. Mineral Dust and Biomass Burning Aerosols, and Their Mixing

[28] A summary of the mean elemental concentrations of the major constituents (Na, Mg, Al, Si, P, S, K, Ca, Ti, and Fe) observed at the ground and on the aircraft during the field campaigns is shown in Table 1. For sake of comparison with published data, elemental ratios with respect to Al are also shown. Mean values for ground-based and aircraft samples are similar. Higher mean concentrations and variability were obtained for the DODO2 campaign because of an extremely intense dust storm which was sampled on 23 August 2006.

[29] As demonstrated by *Osborne et al.* [2008] and *Johnson et al.* [2008], in wintertime the atmospheric column over western Africa was characterized by a multilayer aerosol structure. During winter dust was found close to the surface owing to transport at low level by the Harmattan winds, whereas persistent layers of biomass burning (BB) were found aloft, between 2 and 6 km. Conversely, dust was transported at few-km altitude in summertime [*McConnell et al.*, 2008].

[30] On the basis of visual observations and online monitoring of the spectral behavior of aerosol scattering coefficient available on board the BAe-146, we were able to collect filter samples from layers representing different aerosol conditions.

[31] Dust was found ubiquitously in all of them, including in the elevated BB layers. Evidence for this is in the PIXE spectra for low-Z elements, where the signals of Al and Si were evident together with that of S and K, good tracers for aged BB [*Gaudichet et al.*, 1995; *Ruellan et al.*, 1999]. As a matter of fact, because of their large mass and despite their little number, crustal particles dominated the mass concentrations over biomass burning aerosols, which were numerous but small.

[32] Nevertheless, the relative contribution of mineral dust to the total aerosol load changed with aging of air masses. This effect is clear when looking at the linear correlation between elemental K and Al (Figure 1) for aircraft samples collected in dust layers, fresh BB layers (that is, within aircraft overpass of a smoke plume), and in the elevated BB layers. Only four samples were collected in fresh biomass burning. With this limitation in mind, the K-to-Al ratio was similar for fresh biomass burning and dust layers (0.16–0.18) and close to previous values obtained for mineral dust ($\sim$0.2 [*Chiapello*, 1996; *Formenti et al.*, 2003]) and to the crustal reference value (0.3) of *Mason* [1966]. The ratio was higher (K-to-Al = 0.52) in the elevated biomass burning layers, likely due to the depletion of the coarse mode mineral dust particles during transport and uplift in the atmosphere. As a consequence, the relative

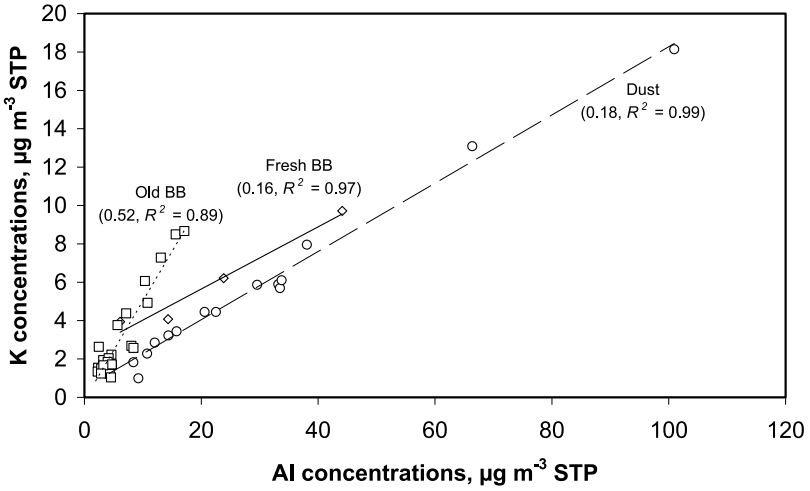

Figure 1. Scatterplot of elemental concentrations of K and Al measured on board the BAe-146 aircraft during the AMMA SOP0/DABEX campaign. Data have been sorted by aerosol type: dust (circles), old BB (squares), and fresh BB (diamonds). The slope of the regression line and the square of the correlation coefficient (R^2) are shown in parentheses.

contribution of fine mode K-containing particles became more significant. Similar ratios have been found previously in smoke from smoldering biomass burning [e.g., *Gaudichet et al.*, 1995; *Ruellan et al.*, 1999].

[33] To illustrate the relative contribution of dust and BB to the aerosol load, we estimated the dust mass (D_M) as sum of the major oxides (Na_2O, MgO, Al_2O_3, SiO_2, K_2O, CaO, TiO_2 and Fe_2O_3), and the BB aerosol mass (BB_M) from measured total carbon (TC). Of course, this is a lower limit for BB_M. An upper limit, taking into account the oxygen and hydrogen associated with organic matter as well as the inorganic fraction, was estimated to be 1.3 × TC by taking literature values of BC/TC, OC/TC and POM/OC [*Ruellan et al.*, 1999].

[34] With these values, we found that the contribution of mineral dust to the aerosol mass load was overwhelming, independently on the nature of the observed air mass. The percent contribution of D_M ranged from 93 (±7) % in dust layers to 72 (±16) % in the elevated BB layers. The percent contribution of D_M in fresh BB was 91 (±9) %, as in dust layers. That is consistent with visual observations during flights, showing that several tenuous smoke plumes from localized small fires diffused almost vertically into a widespread regional haze, mainly composed of mineral dust. The regional character of this persistent and diffuse dust haze is testified also by the fact that debris of fossil diatoms were observed on almost all the filters collected in the surface BB layers, despite the fact that their major source, the Bodélé depression, was not always active during the measurement period. The contribution of mineral dust to the column aerosol load seemed therefore to be rather uniform in the boundary layer, and only decreased in the layers above.

[35] These observations are contrasting to those of *Ruellan et al.* [1999], who found that, during the fire season, mineral dust accounted for only up to 37% of the aerosol mass in the boundary layer over Ivory Coast, around 4°N, that is, south of the Intertropical Convergence Zone (ITCZ), which is at approximately 8°N at the ground at this time of the year. All our observations have been performed above 8°N.

[36] Finally, the question can now be asked about mixing. The investigation by electron microscopy of several filter samples collected in mineral dust, fresh and aged biomass burning layers (not shown), are consistent in suggesting that dust and biomass burning aerosols were externally mixed. *Chou et al.* [2008] have shown that biomass burning aerosols in dust layers are essentially K-S particles in the 0.1–0.6 μm diameter range, whereas mineral dust particles are seldom found below 0.4 μm diameter. These observations match those of *Johnson et al.* [2008] based on analysis of particle number size spectra from optical counting.

[37] External mixing is consistent with the fact that *Johnson et al.* [2008] and *Osborne et al.* [2008] were able to deduce the optical properties of either mineral dust or biomass burning aerosols by linearly deconvoluting measurements performed in mixed layers.

[38] Although electron microscopy performed under vacuum is not suitable to investigate coatings of organic materials, it is worth mentioning that no evidence for organic coating of dust particles could be observed in any of the many samples investigated. On the contrary, transmission electron microscopy yields examples of sulfate coatings on soot particles (not shown). Coatings of mineral dust by organic carbon will be addressed more systematically in future work.

3.2. Elemental Composition of Mineral Dust, Including Regional Variability

[39] In this section we investigate the elemental composition of mineral dust. To make sure to avoid contamination, we only selected samples for which Al concentrations were higher than 20 $\mu g\ m^{-3}$.

[40] Regarding ground-based samples, *Rajot et al.* [2008] were able to isolate eighteen episodes of dust on the basis of the correlation between mass and number concentrations. Five of these episodes were of local origin; the remaining

Table 2. Mean Elemental Composition of Mineral Dust[a]

	Banizombou (Local)		Banizoumbou (Advected)	
	Mean (±std)	Variability (%)	Mean (±std)	Variability (%)
Na	0.9 (0.6)	65	1.1 (0.7)	62
Mg	2.1 (0.1)	7	3.0 (0.4)	15
Al	21.4 (0.6)	3	19 (2)	11
Si	53.5 (0.6)	1	54 (3)	4
K	3.6 (0.2)	7	3.5 (0.3)	10
Ca	4.6 (0.5)	10	7.5 (1.6)	21
Ti	2.3 (0.1)	3	1.4 (0.2)	15
Fe	12.3 (0.3)	3	10.9 (0.9)	9
	AMMA SOP0/DABEX		DODO2 (B238)	
	Mean (±std)	Variability (%)	Mean (±std)	Variability (%)
Na	1.0 (0.4)	43	1.4 (0.1)	8
Mg	2.2 (0.2)	10	3.4 (0.4)	14
Al	20 (2)	8	19 (1)	5
Si	51 (2)	3	46 (1)	3
K	3.6 (0.2)	5	5.3 (0.1)	3
Ca	9.1 (0.5)	6	11 (2)	19
Ti	1.6 (0.2)	11	1.6 (0.1)	7
Fe	11.6 (0.6)	5	12.7 (0.6)	5

[a]Mean elemental composition of mineral dust: (top) episodes of local emission and advected dust observe at the ground-based site of Banizoumbou (Niger) and (bottom) on board the BAe-146 during the AMMA SOP0/DABEX wintertime field phase over Niger and flight B238 during the DODO2 summertime field phase over Mauritania. Standard deviation (abbreviated as std) around the mean value is shown in parentheses. The percent variability (standard deviation/mean) of the composition is also shown.

thirteen corresponded to dust advected from more distant sources. By coupling a statistical analysis (Principal Component Analysis (PCA)) of the temporal covariance of the elemental concentrations and calculated five-day back trajectories, *Rajot et al.* [2008] were also able to show that the various episodes of advected dust had originated from different source regions.

[41] Thirteen filters were retained during episodes of advected dust and five during episodes of local production. For each of these samples, we calculated the mean composition of mineral dust as percent of the total mass estimated as sum of the measured concentrations for Na, Mg, Al, Si, K, Ca, Ti and Fe. These results are presented in Table 2.

[42] We first investigate ground-based data. The mean composition obtained for locally produced dust is 21.4% (±0.6) for Al, 53.4 (±0.6) for Si, 12.3% (±0.3) for Fe, 4.6% (±0.5) for Ca, 3.6% (±0.2) for K, 2.3% (±0.1) for Ti, 2.1% (±0.1) for Mg, and 0.9% (±0.1) for Na. Beside Na, which was above analytical detection limit only on two of the 5 samples, little variability (within 10%) was observed from sample to sample.

[43] The mean composition obtained for advected dust is 19% (±2) for Al, 54 (±3) for Si, 10.9% (±0.9) for Fe, 7.5% (±1.6) for Ca, 3.5% (±0.3) for K, 1.4% (±0.2) for Ti, 3.0% (±0.4) for Mg, and1.1% (±0.7) for Na. One can immediately note that the percent variability on each of the components is much larger (up to 21% for Ca).

[44] Furthermore, the composition of locally produced and advected dust is similar, yet different. Si is ubiquitous and found in identical proportions. On the contrary, locally produced dust has lower Ca and Mg contents, but higher Al, Fe and Ti than advected dust. A *t*-test confirms that these differences are not speculative but have statistical significance (95% significance level).

[45] The enrichment of local dust in Al, Fe and Ti is in agreement with the expected composition of Sahelian dust, dominated by calcium-poor clays, mainly kaolinite ($Al_4[Si_4O_{10}](OH)_8$) but also illite (($K_{0.7}$, $Na_{0.2}$, $Ca_{0.1}$)(Al_3, $Fe_{0.6}$, $Mg_{0.4}$)(Si_7, Al)$O_2(OH)_4$) [*Caquineau et al.*, 1998], as well as iron-oxides such as hematite and goethite. The good correlation between Al, Fe and Ti ($R^2 = 0.79$ and $R^2 = 0.76$, for Fe versus Al and Ti versus Al, respectively) suggests that Fe and Ti are associated with clays. Fe is found in the crystalline lattice of clays, but also as iron oxides (such as hematite/goethite, Fe_2O_3/FeO-OH respectively), in the form of little spheres on the surface of clay particles [*Lafon et al.*, 2006]. Ti oxides such as anatase (TiO_2) are also found in mineral dust in association with clays. As a matter of fact, small individual particles of Ti and iron oxides were observed by electron microscopy on some of the aircraft filters [*Chou et al.*, 2008]. Conversely, the advected dust is marked by enrichment in Ca and Mg. These elements were correlated ($R^2 = 0.67$). Carbonates such as calcite ($CaCO_3$) and dolomite ($CaMg(CO_3)_2$) are found in the North African deserts of Libya, Algeria, and Tunisia, thus calcium is a good tracers for Saharan dust [*Lafon et al.*, 2006].

[46] We can now explore the variability in the mean composition of the advected dust which could be due to the different origin of the various episodes [*Rajot et al.*, 2008]. To do so, we sorted the percent composition of each of the episodes accordingly to their Ca-content. Because Ca showed the largest percent variability (ranging from 5.3 to 10.1% of the estimated dust mass), this allows maximizing sample-to-sample differences. Each sample was associated at the corresponding five-day back trajectory. When doing so, samples having Ca content lower than 7% seemed to associate with air masses from within Niger, whereas samples for which the Ca percent value was larger than 7% rather associated with transport from Algeria, Libya and western Africa/Morocco. One sample (SOP0-4) is peculiar. This corresponded to the outbreak of mineral dust from the Bodélé depression that had also been detected by the lidar system installed in Banizoumbou [*Heese and Wiegner*, 2008]. The identification of the Bodélé as the source region is unequivocal owing to the numerous diatoms debris that appeared on the electron microscope images. Bodélé has been shown to be the major source region of such diatoms [*Washington et al.*, 2006]. The composition of the sample attributed to the Bodélé source is significantly different (*t*-test, 95% significance level) from that of the other episodes, except that for Ca and Mg. In particular, the samples from Bodélé had the highest Si content (60%), signature of the fossil diatoms, and the lowest Al, K, and Fe content (15, 3.1 and 8.9%, respectively).

[47] This analysis was extended to the aircraft samples. Nine aircraft samples were retained for the AMMA SOP0/DABEX phase, which were collected mainly during three dedicated flights [*Osborne et al.*, 2008; *Chou et al.*, 2008], but also during straight and leveled runs (SLRs) of opportunity. Twelve samples were retained for DODO, 4 from DODO1 and the remaining 8 from DODO2. The DODO2 samples were mainly collected during two severe dust storms from western Sahara and Morocco [*McConnell et al.*, 2008].

[48] The mean composition of aircraft samples collected over Niger during AMMA SOP0/DABEX is 20% (±2) for Al, 51 (±2) for Si, 11.6% (±0.6) for Fe, 9.1% (±0.5) for Ca, 3.6% (±0.2) for K, 1.6% (±0.2) for Ti, 2.2% (±0.2) for Mg, and 1.0% (±0.4) for Na. This is rather consistent with the mean composition obtained for advected dust from the ground-based samples. However, aircraft samples have less Si and Mg and more Ca, Ti, and Fe than the ground-based ones (*t*-test, 95% significance level). Artifacts, such as different sampling efficiencies of the aircraft and ground-based sampling inlets or efficiencies of analytical techniques, might provoke these differences. However, we do not expect them to be major. In fact we compared the number size distributions measured on the aircraft and at the ground during aircraft overpasses at low altitude (300 m above ground level) and found that is compared remarkably well over the region of overlap (0.3–3 μm diameter) of the particle counters operated airborne and ground-based. As it will be shown in section 3.3, differences in composition between ground-based and aircraft samples correspond to real mineralogical differences in the sampled dust. As a matter of fact, the aircraft did not fly during any of the episodes detected at Banizoumbou, except on 1 February, when the dust composition from ground-based and aircraft sampling is consistent.

[49] The DODO sample composition was similar than that of AMMA SOP0/DABEX. The exception was the mean composition of the dust storm which was encountered during flight B238 (23 August 2006). The mean percent composition obtained from three samples is 19% (±1) for Al, 46% (±1) for Si, 12.7% (±0.6) for Fe, 11% (±2) for Ca, 5.3% (±0.1) for K, 1.6% (±0.1) for Ti, 3.4% (±0.4) for Mg, and 1.4% (±0.1) for Na.

[50] The dispersion in the Ca values might reflect the contribution of air masses from different source regions that appeared to be at different heights [*McConnell et al.*, 2008]. Differences with respect to the mean AMMA SOP0/DABEX dust composition (excluding the Bodélé sample) are observed for Si, Fe, Ca, Mg, and, for the first time, for K. This is consistent with the enrichment in K-bearing illite clays with respect to kaolinite expected between western Africa and the Sahel [*Caquineau et al.*, 2002], which also became apparent from the XRD analysis (see section 3.3). Electron microscope observations also indicated that dust aerosols collected during B238 flight (and during the DODO experiment in general) were often complex aggregates containing K, whereas were mostly simple aluminosilicates made of Al, Si and Fe over Niger [*Chou et al.*, 2008]. The high sample-to-sample variability prevents any conclusions regarding a possible enrichment in Na. This was observed during previous sampling in the region [*Formenti et al.*, 2003], either because of mixing with sea breeze or as mineral halite (NaCl), which is one of the soil constituents of the local source regions, often dried saline lake deposits. Na was often observed by electron microscopy in many of the particles investigated.

3.3. Mineralogical Composition of Mineral Dust

[51] These results are in agreement with the observations by X-ray diffraction analysis (XRD), which could be performed on almost all the samples discussed in the previous section. For each sample, results are shown in Figure 2 (top) in terms of the percent of total diffracted peak surface of the XRD spectra due to the different minerals in the crystallized phase. Figure 2 (bottom) shows the ratio of the percent total diffracted surface of illite and kaolinite. *Caquineau et al.* [1998] has shown that this ratio is sensitive to the source of provenance of African mineral dust.

[52] There is some consistency in the mineralogical signature from sample to sample. Clays (kaolinite and illite) accounted for 50–60% of the measured signal, quartz for about 30–40%, K-feldspar and plagioclase (feldspar containing Na and Ca) for about 5%, and carbonate (calcite, dolomite and gypsum) for the remaining 10–15%. The largest fluctuations are observed again on the carbonate fraction, calcite in particular, which is greatly enriched (up to 20–30% of the signal) on some of the samples collected during AMMA SOP0/DABEX. The simultaneous detection of palygorskite at trace level (not shown) suggests that dust likely originated from North Africa (east of Egypt or Algeria). The dust collected during DODO2 (flight B238) has a rather similar composition. However, more subtle differences become evident when looking at the illite/kaolinite ratio. Dust collected over Niger (samples collected at the ground and during AMMA SOP0/DABEX) are characterized by an illite/kaolinite ratio of the order of 0.1–0.3, dust collected over Mauritania appears to be richer in illite (ratio of the order of 0.6). This is consistent with previous findings by *Caquineau et al.* [2002].

[53] We must warn the reader on the fact that the percent of total diffracted surface cannot be used readily to infer the mass concentrations of the various minerals. First of all, not all the collected aerosol mass is analyzed. In fact, in order to reduce the detection limit of the technique, the aerosol deposited on the filter needs to be placed on a specific sample holder. To do so, a fraction of the original sample is used, which, in spite of the degree of precision in manipulation, may not be identical from sample to sample. Second, the XRD signal (the total diffracted peak surface) is due to the crystalline fraction only of the aerosol, and not to the total dust mass. This fraction might vary from sample to sample, as it is illustrated in Figure 3 by the scatterplot of the total diffracted peak surface of the ground-based samples versus the analyzed mass. The correlation is satisfactory ($R^2 = 0.64$); however, the large scatter indicates that the fraction of diffracting material is not strictly equal from sample to sample. As an example, the total diffracted peak surface for sample SOP0-4 (circle) is lower by a factor of 3 than that of sample SOP0-29 (triangle), in spite of the fact that the analyzed mass is the same. Sample SOP0-4 was collected during the Bodélé outbreak and contained a large percent of amorphous diatoms debris.

[54] For a given mineral, the presence of amorphous phases (e.g., diatoms debris) prevents us from quantifying the crystalline fraction from the mass elemental concentration measured by XRF. Another difficulty is due to the fact that the same element might be present in various minerals. This is the case for quartz, which does not correlate with the silicon (percent of total oxide mass from elemental analysis). The clay fraction (illite + kaolinite) fraction did not correlate with the aluminum fraction either, likely because the Al content of each of these different species is different. Conversely, good correlation ($R^2 = 0.63$) is found between the crystalline calcium fraction (calcite + dolomite) and

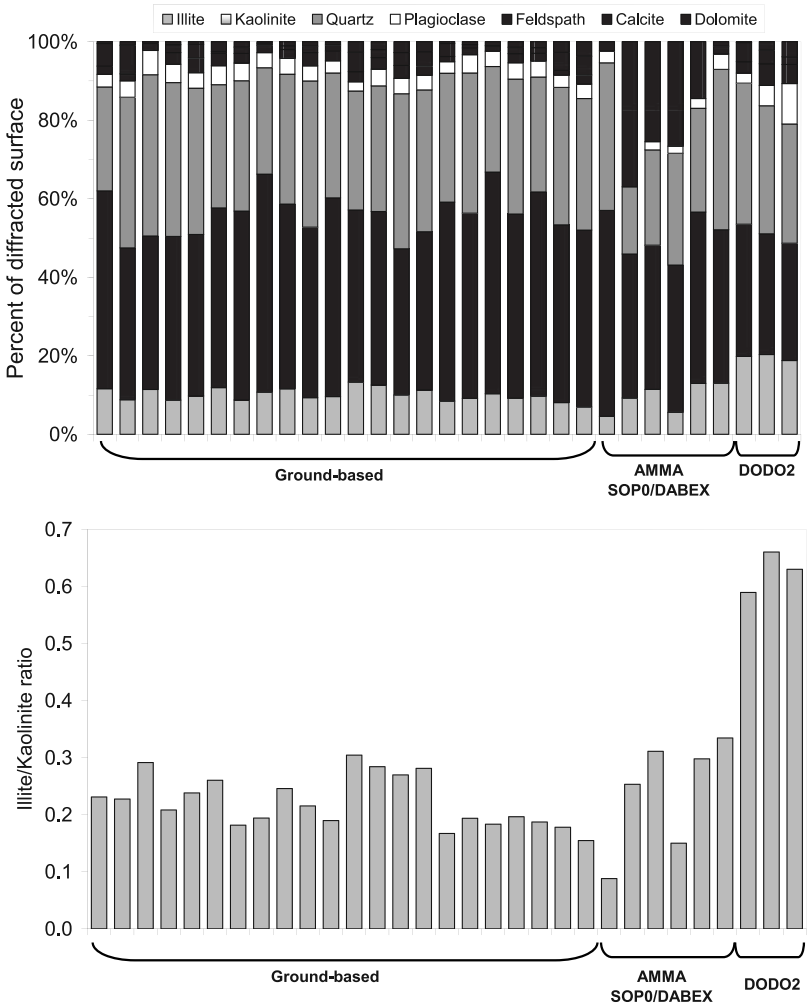

Figure 2. (top) Percent of the total diffracted peak surface obtained by X-ray diffraction (XRD) analysis for various minerals detected in ground-based and aircraft samples and (bottom) corresponding illite-to-kaolinite ratios.

elemental calcium, suggesting that all the elemental calcium is in the crystalline form (Figure 4).

[55] Finally, the iron-oxide content and mineralogy (speciation hematite and goethite) was investigated. The iron-oxide content could be measured on fourteen ground-based samples, three collected during episodes of advection and one during an episode of local emission. The mean ratio of iron oxide-to-total elemental iron was 59% (±5), and varied between 52% and 63%. The lowest value was found for sample SOP0-4 corresponding to the Bodélé dust outbreak, while the highest value corresponds to the episode of local production (SOP0-46). Our values are in agreement with those reported for Niger dust by *Lafon et al.* [2006] for advection (43% (±10)) and dust from local erosion (65% (±5)). The iron-oxide content varied between 2.4% and 4.5% of the total estimated dust mass (expressed as sum of oxides); again the maximum and minimum values corresponding to dust from Bodélé and dust emitted by local erosion. These values agree with those of *Lafon et al.* [2006], who found 2.8% (±0.8) and 5.0% (±0.4) for advected and locally emitted dust, respectively. Some differences might be due to the fact that we did not estimated the total dust mass in the same way.

[56] Six aircraft samples could be analyzed, five for dust over Niger and one for dust over Mauritania. Results are consistent with those obtained on the ground. The iron oxide-to-Fe ratio varied between 46 and 59%. The lowest iron oxide-to-Fe ratio is obtained for dust originated from northern Africa, whereas the highest value is obtained for sample B238 collected over Mauritania, where iron mining is extensive. This information is resumed in Figure 5 showing the iron oxide-to-Fe ratio as a function of the percent content of total iron in the total estimated dust mass (as sum of oxides).

[57] Finally, spectral diffuse reflectance analysis performed on those samples indicated that iron oxides were composed by relative proportions of hematite and goethite in relatively constant proportions (30% and 70%, respectively). This is in accordance with previous findings [*Lafon et al.*, 2006]. The Bodélé sample had no measureable signal. The iron oxide depletion in Bodélé dust is apparent.

4. Summary of Conclusions

[58] In this paper we presented results on the elemental and mineralogical composition of samples of mineral dust

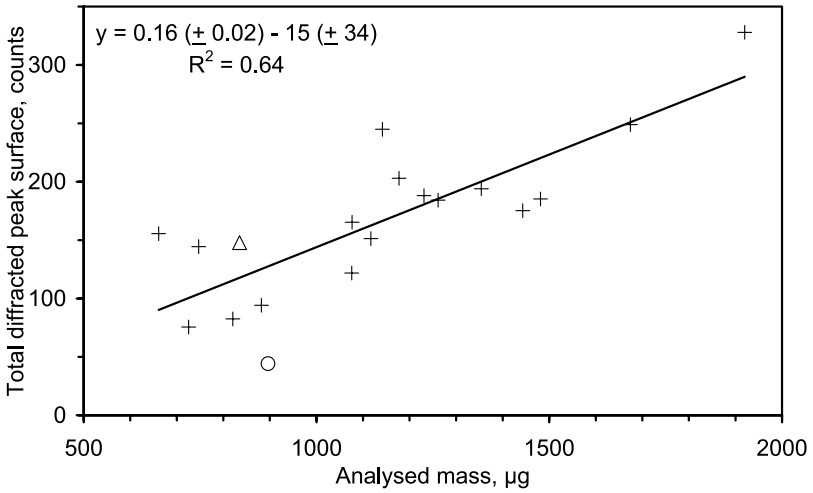

Figure 3. Scatterplot of the total diffracted peak surface obtained by X-ray diffraction (XRD) analysis of the ground-based samples versus the aerosol mass analyzed by the technique. The total diffracted peak surface represents the total XRD signal provided by the fraction of the aerosols which is in the crystalline form. The total diffracted peak surface for sample SOP0-4 (circle), collected during the Bodélé outbreak of 15 January 2006, is lower by a factor of 3 than that of sample SOP0-29 (triangle), in spite of the fact of that the analyzed mass is the same.

collected during January–February and August 2006 over Niger and Senegal, in western Africa, during three of the ground-based and airborne field phases of the AMMA and DODO projects.

[59] Within the limit of the sampling statistics, and the experimental and analytical uncertainties, ground-based and airborne measurements provided a valuable and consistent data set to investigate the composition of mineral dust from different source regions.

[60] First of all, our data (ground-based and airborne) indicate that in wintertime mineral dust dominated the aerosol mass load at the regional scale at latitudes north than 8°N. Mineral dust accounted for 72% to 93% of the aerosol mass, the lower limit being found in layers enriched in biomass burning aerosols and transported in the free troposphere. Active fires were observed in Nigeria and Benin. Mineral dust and biomass burning aerosols were externally mixed, and occurred in different size ranges. This has important implications for the calculation of optical and radiative properties of the resulting aerosols.

[61] Our data testify of the variability of dust composition according to source region of emission. The clay assemblage was rather consistent for all the samples (high kaolinite content with respect to illite), resulting in illite-to-kaolinite ratio between 0.2 and 0.6. The upper limit corresponded to samples collected over Mauritania. High kaolinite content associated to illite also characterizes Australian dust [*Kiefert et al.*, 1996], whereas illite-to-

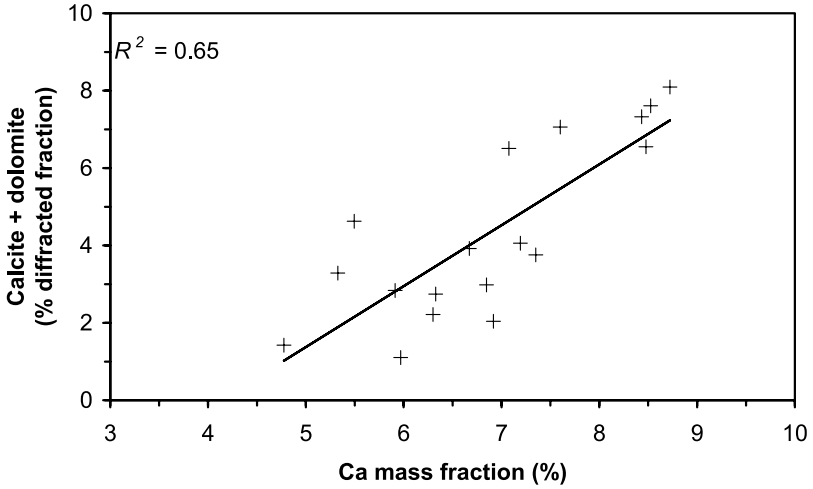

Figure 4. Scatterplot of the crystalline calcium fraction (calcite + dolomite) and the Ca mass fraction (percent of the total mass estimated from elemental analysis), suggesting that all the elemental calcium is in the crystalline form.

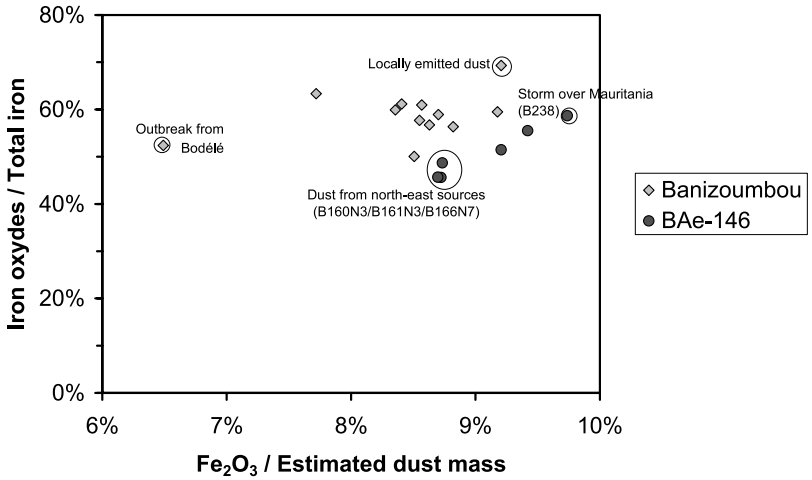

Figure 5. Scatterplot of the iron oxide-to-Fe ratio and the percent content of Fe in the total estimated dust mass for samples collected at Banizoumbou (diamonds) and on board the BAe-146 during AMMA SOP0/DABEX, DODO1, and DODO2 (circles). Samples with contrasted iron oxide-to-Fe ratio are highlighted.

kaolinite ratio above 1 is expected in dust from northern deserts (Morocco, Tunisia, and northern Algeria) [*Caquineau et al.*, 2002], but also of higher-latitude desert areas in Asia [e.g., *Biscaye et al.*, 1997; *Svensson et al.*, 2000].

[62] Variability was observed in the calcium and iron contents, and their mineralogical speciation. Calcite and dolomite were enriched in dust transported from deserts of north Africa (likely Egypt), whereas iron oxides were enriched in dust emitted locally from Niger and Mauritania, but depleted in dust transported from the Bodélé depression.

[63] On the contrary, indications are that the relative proportions of hematite and goethite (Fe_2O_3 and FeO-OH, respectively), the two major iron oxides in mineral dust, are independent of the source region of emission.

[64] Various authors [e.g., *Sokolik and Toon*, 1999; *Alfaro et al.*, 2004; *Lafon et al.*, 2006] have illustrated the importance of iron oxides in controlling the absorption properties of mineral dust in the visible spectrum. The imaginary part of the refractive index of hematite and goethite ranges between 0.1 and 3, respectively, at wavelengths lower than 1 μm. The other major minerals in mineral dust, clays (illite and kaolinite), quartz and calcite are only little absorbing, their imaginary part remaining below 0.001 across the visible spectrum. For a given size distribution, the iron oxide content and mineralogy are expected to rule the absorption properties of mineral dust.

[65] Because the magnitude but also the spectral dependence of the imaginary part of the refractive index of hematite and goethite are different, accurate determination of their respective content must be undertaken in order to model their optical properties realistically. To our knowledge, to date only one study has tempted to do so. On the basis of experimental data of the content and mineralogy of iron oxides, *Lafon et al.* [2006] have calculated the single scattering albedo for mineral dust aerosols produced in a laboratory wind tunnel for soils from various source regions (Niger, Tunisia, and China), and found that the single scattering albedo across the visible spectrum should be of the order of 0.8 and 0.9 for a Niger aerosol, whereas the single scattering albedo of aerosols from China and Tunisia, having a lower iron oxide content, should vary between 0.9 and 0.95. These values might not be readily transposed to our data, because of the differences in the number size distribution between airborne and wind-tunnel generated aerosols. Transported aerosols such as those observed in the wintertime during AMMA should have a less important coarse fraction than aerosols generated in a wind tunnel.

[66] As a consequence, careful modeling of the spectral refractive index and single scattering albedo of the AMMA aerosols, taking into account the measured mineralogical composition and number size distribution, will be undertaken shortly.

[67] **Acknowledgments.** Based on a French initiative, AMMA was built by an international scientific group and is currently funded by a large number of agencies, especially from France, the United Kingdom, the United States, and Africa. It has been the beneficiary of a major financial contribution from the European Community's Sixth Framework Research Programme. Detailed information on scientific coordination and funding is available on the AMMA International Web site at http://www.amma-international.org. Financial support of the API-AMMA and LEFE (project BIRD) national programs is acknowledged. The authors also wish to thank the BAe-146 air and ground crews, as well as the FAAM and Met Office observers. H. Cachier and K. Oikonomou (LSCE, Gif sur Yvette, France) provided the analysis of total carbon. K. Djabaku (LISA) and L. Galoisy (IMPCM) are thanked for helping with diffuse reflectance analysis. S. Lafon (LISA) is thanked for useful discussion.

References

Alfaro, S. C., S. Lafon, J. L. Rajot, P. Formenti, A. Gaudichet, and M. Maillé (2004), Iron oxides and light absorption by pure desert dust: An experimental study, *J. Geophys. Res.*, *109*, D08208, doi:10.1029/2003JD004374.

Andreae, M. O., H. Berresheim, T. W. Andreae, M. A. Kritz, T. S. Bates, and J. T. Merrill (1988), Vertical distribution of dimethylsulfide, sulfur dioxide, aerosol ions, and radon over the northeast Pacific Ocean, *J. Atmos. Chem.*, *6*, 149–173, doi:10.1007/BF00048337.

Andreae, M. O., W. Elbert, R. Gabriel, D. W. Johnson, S. Osborne, and R. Wood (2000), Soluble ion chemistry of the atmospheric aerosol and SO_2 concentrations over the eastern North Atlantic during ACE-2, *Tellus, Ser. B*, *52*, 1066–1087, doi:10.1034/j.1600-0889.2000.00105.x.

Biscaye, P. E., F. E. Grousset, M. Revel, S. Van der Gaasr, G. A. Zielinski, A. Vaars, and G. Kukla (1997), Asian provenance of glacial dust (stage 2) in GISP2 ice core, Summit, Greenland, *J. Geophys. Res.*, *102*, 26,765–26,781, doi:10.1029/97JC01249.

Calzolai, G., M. Chiari, I. García Orellana, F. Lucarelli, A. Migliori, S. Nava, and F. Taccetti (2006), The new external beam facility for

environmental studies at the Tandetron accelerator of LABEC, *Nucl. Instrum. Methods Phys. Res., Sect. B*, *249*, 928–931, doi:10.1016/j.nimb.2006.03.193.

Caquineau, S., M.-C. Magonthier, A. Gaudichet, and L. Gomes (1997), An improved procedure for the X-ray diffraction analysis of low-mass atmospheric dust samples, *Eur. J. Mineral.*, *9*, 157–166.

Caquineau, S., A. Gaudichet, L. Gomes, M.-C. Magonthier, and B. Chatenet (1998), Saharan dust: Clay ratio as a relevant tracer to assess the origin of soil-derived aerosols, *Geophys. Res. Lett.*, *25*, 983–986, doi:10.1029/98GL00569.

Caquineau, S., A. Gaudichet, L. Gomes, and M. Legrand (2002), Mineralogy of Saharan dust transported over northwestern tropical Atlantic Ocean in relation to source regions, *J. Geophys. Res.*, *107*(D15), 4251, doi:10.1029/2000JD000247.

Chiapello, I. (1996), Les aérosols atmosphériques au-dessus de l'Atlantique nord tropical: Approche physico-chimique et météorologique. Evaluation de la contribution des différentes espèces à l'épaisseur optique en aérosol, Ph.D. thesis, Univ. Paris VII, Paris.

Chou, C., P. Formenti, M. Maille, P. Ausset, G. Helas, M. Harrison, and S. Osborne (2008), Size distribution, shape, and composition of mineral dust aerosols collected during the African Monsoon Multidisciplinary Analysis Special Observation Period 0: Dust and Biomass-Burning Experiment field campaign in Niger, January 2006, *J. Geophys. Res.*, *113*, D00C10, doi:10.1029/2008JD009897.

Claquin, T., M. Schulz, and Y. J. Balkanski (1999), Modeling the mineralogy of atmospheric dust sources, *J. Geophys. Res.*, *104*, 22,243–22,256, doi:10.1029/1999JD900416.

de Reus, M., F. Dentener, A. Thomas, S. Borrmann, J. Ström, and J. Lelieveld (2000), Airborne observations of dust aerosols over the North Atlantic Ocean during ACE-2: Indications for heterogeneous ozone destruction, *J. Geophys. Res.*, *105*, 15,263–15,275, doi:10.1029/2000JD900164.

Dentener, F. J., G. R. Carmichael, Y. Zhang, J. Lelieveld, and P. J. Crutzen (1996), Role of mineral aerosol as a reactive surface in the global troposphere, *J. Geophys. Res.*, *101*, 22,869–22,889, doi:10.1029/96JD01818.

Faye, G. H. (1968), The optical spectra of six coordinate sites in chlorite, biotite, phlogopite and vivianite: Some aspects of pleochroism in the sheet silicates, *Can. Mineral.*, *9*, 403–425.

Formenti, P., W. Elbert, W. Maenhaut, J. Haywood, and M. O. Andreae (2003), Chemical composition of mineral dust aerosol during the Saharan Dust Experiment (SHADE) airborne campaign in the Cape Verde region, September 2000, *J. Geophys. Res.*, *108*(D18), 8576, doi:10.1029/2002JD002648.

Forster, P., et al. (2007), Changes in atmospheric constituents and in radiative forcing, in *Climate Change 2007: The Physical Science. Contribution of Working Group I to the Fourth Assessment Report of the Intergovernmental Panel on Climate Change*, edited by S. Solomon et al., pp. 131–234, Cambridge Univ. Press, Cambridge, U.K.

Gaudichet, A., F. Echalar, B. Chatenet, J. P. Quisefit, G. Malingre, H. Cachier, P. Buat-Menard, P. Artaxo, and W. Maenhaut (1995), Trace elements in tropical African savanna biomass burning aerosols, *J. Atmos. Chem.*, *22*, 19–39, doi:10.1007/BF00708179.

Haywood, J. M., et al. (2008), Overview of the African Multidisciplinary Monsoon Analysis Special Observational Period 0 and the Dust and Biomass Burning Experiment, *J. Geophys. Res.*, doi:10.1029/2008JD010077, in press.

Heese, B., and M. Wiegner (2008), Vertical aerosol profiles from Raman polarization lidar observations during the dry season AMMA field campaign, *J. Geophys. Res.*, *113*, D00C11, doi:10.1029/2007JD009487.

Hinds, W. C. (1982), *Aerosol Technology: Properties, Behavior, and Measurement of Airborne Particles*, 424 pp., John Wiley, Toronto, Canada.

Hudson, P. K., E. R. Gibson, M. A. Young, P. D. Kleiber, and V. H. Grassian (2008), Coupled infrared extinction and size distribution measurements for several clay components of mineral dust aerosol, *J. Geophys. Res.*, *113*, D01201, doi:10.1029/2007JD008791.

Jickells, T. D., et al. (2005), Global iron connections between desert dust, ocean biogeochemistry, and climate, *Science*, *308*, 67–71, doi:10.1126/science.1105959.

Johnson, B. T., S. R. Osborne, J. M. Haywood, and M. A. J. Harrison (2008), Aircraft measurements of biomass burning aerosol over West Africa during DABEX, *J. Geophys. Res.*, *113*, D00C06, doi:10.1029/2007JD009451.

Karickhoff, S. W., and G. W. Bailey (1973), Optical absorption spectra of clay minerals, *Clays Clay Miner.*, *21*, 59–70, doi:10.1346/CCMN.1973.0210109.

Kiefert, L., G. H. Mc Tainsch, and W. G. Nickling (1996), Sedimentological characteristics of Saharan and Australian dusts, in *The impact of Desert Dust across the Mediterranean*, edited by S. Guerzoni and R. Chester, pp. 183–190, Kluwer Acad., Dordrecht, Netherlands.

Lafon, S., J. L. Rajot, S. C. Alfaro, and A. Gaudichet (2004), Quantification of iron oxides in desert aerosols, *Atmos. Environ.*, *38*, 1211–1218, doi:10.1016/j.atmosenv.2003.11.006.

Lafon, S., I. N. Sokolik, J. L. Rajot, S. Caquineau, and A. Gaudichet (2006), Characterization of iron oxides in mineral dust aerosols: Implications for light absorption, *J. Geophys. Res.*, *111*, D21207, doi:10.1029/2005JD007016.

Mason, B. (1966), *Principles of Geochemistry*, 3rd ed., John Wiley, New York.

Maxwell, J. A., W. J. Teesdale, and J. L. Campbell (1995), The Guelph PIXE software package II, *Nucl. Instrum. Methods Phys. Rev., Sect B*, *95*, 407–421, doi:10.1016/0168-583X(94)00540-0.

McConnell, C. L., E. J. Highwood, H. Coe, P. Formenti, B. Anderson, S. Osborne, S. Nava, K. Desboeufs, G. Chen, and M. A. J. Harrison (2008), Seasonal variations of the physical and optical characteristics of Saharan dust: Results from the Dust Outflow and Deposition to the Ocean (DODO) experiment, *J. Geophys. Res.*, *113*, D14S05, doi:10.1029/2007JD009606.

Mehra, O. P., and M. L. Jackson (1960), Iron oxide removal from soils and clays by a dithionite-citrate system buffered with sodium bicarbonate, *Clays Clay Miner.*, *7*, 317–327, doi:10.1346/CCMN.1958.0070122.

Moreno, T., X. Querol, S. Castillo, A. Alastuey, E. Cuevas, L. Herrmann, M. Mounkaila, J. Elvira, and W. Gibbons (2006), Geochemical variations in aeolian mineral particles from the Sahara-Sahel Dust Corridor, *Chemosphere*, *65*, 261–270, doi:10.1016/j.chemosphere.2006.02.052.

Osborne, S. R., B. T. Johnson, J. M. Haywood, A. J. Baran, M. A. J. Harrison, and C. L. McConnell (2008), Physical and optical properties of mineral dust aerosol during the Dust and Biomass-burning Experiment, *J. Geophys. Res.*, *113*, D00C03, doi:10.1029/2007JD009551.

Queralt, I., T. Sanfeliu, E. Gomez, and C. Alvarez (2001), X-ray diffraction analysis of atmospheric dust using low-background supports, *J. Aerosp. Sci.*, *32*, 453–459, doi:10.1016/S0021-8502(00)00090-2.

Rajot, J. L., et al. (2008), AMMA dust experiment: An overview of measurements performed during the dry season special observation period (SOP0) at the Banizoumbou (Niger) supersite, *J. Geophys. Res.*, doi:10.1029/2008JD009906, in press.

Ramanathan, V., P. J. Crutzen, J. T. Kiehl, and D. Rosenfeld (2001), Aerosols, climate, and the hydrological cycle, *Science*, *294*, 2119–2124, doi:10.1126/science.1064034.

Redelsperger, J. L., C. D. Thorncroft, A. Diedhiou, T. Lebel, D. J. Parker, and J. Polcher (2006), African Monsoon Multidisciplinary Analysis: An international research project and field campaign, *Bull. Am. Meteorol. Soc.*, *87*, 1739–1746, doi:10.1175/BAMS-87-12-1739.

Ruellan, S., H. Cachier, A. Gaudichet, P. Masclet, and J. P. Lacaux (1999), Airborne aerosols over central Africa during the Experiment for Regional Sources and Sinks of Oxidants (EXPRESSO), *J. Geophys. Res.*, *104*, 30,673–30,690, doi:10.1029/1999JD900804.

Salisbury, G., J. Williams, V. Gros, S. Bartenbach, X. Xu, H. Fischer, R. Kormann, M. de Reus, and M. Zöllner (2006), Assessing the effect of a Saharan dust storm on oxygenated organic compounds at Izaña, Tenerife (July–August 2002), *J. Geophys. Res.*, *111*, D22303, doi:10.1029/2005JD006840.

Scheinost, A. C., A. Chavernas, V. Barron, and J. Torrent (1998), Use and limitations of second-derivative diffuse reflectance spectroscopy in the visible range to identify and quantify Fe oxide minerals in soils, *Clays Clay Miner.*, *46*, 528–536, doi:10.1346/CCMN.1998.0460506.

Sokolik, I. N., and O. B. Toon (1999), Incorporation of mineralogical composition into models of the radiative properties of mineral aerosol from UV to IR wavelengths, *J. Geophys. Res.*, *104*, 9423–9444, doi:10.1029/1998JD200048.

Sokolik, I., D. Winker, G. Bergametti, D. A. Gillette, G. Carmichael, Y. Kaufman, L. Gomes, L. Schütz, and J. Penner (2001), Introduction to special section: Outstanding problems in quantifying the radiative impact of mineral dust, *J. Geophys. Res.*, *106*, 18,015–18,027, doi:10.1029/2000JD900498.

Svensson, A., P. E. Biscaye, and F. E. Grousset (2000), Characterization of late glacial continental dust in Greenland Ice Core Project ice core, *J. Geophys. Res.*, *105*, 4637–4656, doi:10.1029/1999JD901093.

Swap, R., M. Garstang, S. Greco, R. Talbot, and P. Kållberg (1992), Saharan dust in the Amazon basin, *Tellus, Ser. B*, *44*, 133–149, doi:10.1034/j.1600-0889.1992.t01-1-00005.x.

Tanré, D., J. Haywood, J. Pelon, J. F. Léon, B. Chatenet, P. Formenti, P. Francis, P. Goloub, E. J. Highwood, and G. Myhre (2003), Measurement and modeling of the Saharan dust radiative impact: Overview of the Saharan Dust Experiment (SHADE), *J. Geophys. Res.*, *108*(D18), 8574, doi:10.1029/2002JD003273.

Washington, R., M. C. Todd, S. Engelstaedter, S. Mbainayel, and F. Mitchell (2006), Dust and the low-level circulation over the Bodélé Depression, Chad: Observations from BoDEx 2005, *J. Geophys. Res.*, *111*, D03201, doi:10.1029/2005JD006502.

Willeke, K., and P. A. Baron (1993), *Aerosol measurement: Principles, Techniques and Applications*, 876 pp., Van Nostrand Reinhold, New York.

S. Alfaro, S. Chevaillier, K. Desboeufs, P. Formenti, A. Gaudichet, E. Journet, and S. Triquet, LISA, Universités Paris 12 et Paris 7, CNRS, 61 Avenue du Général de Gaulle, F-94010 Créteil, France. (formenti@lisa.univ-paris12.fr)

S. Caquineau, UR 055 Paleotropique, Institut de Recherche pour le Développement, 32, Rue Henri Varagnat, F-93143 Bondy CEDEX, France.

M. Chiari and S. Nava, National Institute of Nuclear Physics, I-50019 Florence, Italy.

H. Coe, School of Earth, Atmosphere and Environmental Science, University of Manchester, Manchester M13 9PL, UK.

J. Haywood, Met Office, Fitzroy Road, Exeter EX1 3PB, UK.

E. Highwood, Department of Meteorology, Reading University, Whiteknights, P.O. Box 217, Reading RG6 6AH, UK.

J. L. Rajot, UR 176 Solutions, Institut de Recherche pour le Développement, BP 11416, Niamey, Niger.